Wind and Structures, *Vol. 25, No. 4 (2017) 343-360*
DOI: https://doi.org/10.12989/was.2017.25.4.343

Study on post-flutter state of streamlined steel box girder based on 2 DOF coupling flutter theory

Junfeng Guo[1a], Shixiong Zheng[*1], Jinbo Zhu[1], Yu Tang[2] and Chengjing Hong[1]

[1]*School of Civil Engineering, Southwest Jiaotong University, Chengdu, China, 610031*
[2]*School of Civil Engineering and Architecture, Southwest Petroleum University, Chengdu, China, 610500*

(Received May 25, 2017, Revised August 9, 2017, Accepted August 12, 2017)

Abstract. The post-flutter state of streamlined steel box girder is studied in this paper. Firstly, the nonlinear aerodynamic self-excited forces of the bridge deck cross section were investigated by CFD dynamic mesh technique and then the nonlinear flutter derivatives were identified on this basis. Secondly, based on the 2-degree-of-freedom (DOF) coupling flutter theory, the torsional amplitude and the nonlinear flutter derivatives were introduced into the traditional direct flutter calculation method, and the original program was improved to the "post-flutter state analysis program" so that it can predict not only the critical flutter velocity but also the movement of the girder in the post-flutter state. Finally, wind tunnel tests were set to verify the method proposed in this paper. The results show that the effect of vertical amplitude on the nonlinear flutter derivatives is negligible, but the torsional amplitude is not; with the increase of wind speed, the post-flutter state of streamlined steel box girder includes four stages, namely, "little amplitude zone", "step amplitude zone", "linearly growing amplitude zone" and "divergence zone"; damping ratio has limited effect on the critical flutter velocity and the steady state response in the post-flutter state; after flutter occurs, the vibration form is a single frequency vibration coupled with torsional and vertical DOF.

Keywords: streamlined steel box girder; post-flutter state; soft flutter; CFD; wind tunnel tests

1. Introduction

Recently, as the span of bridge is longer and longer, the modern bridge becomes more slender and flexible, and its damping ratio is getting lower. Therefore, the modern bridge is more and more sensitive to wind, and wind load has become one of the key factors in long-span bridge construction and operation. Flutter is a very dangerous divergence movement among all kinds of wind-induced vibration. Appropriate measures should be taken in the bridge design to avoid flutter.

At present, the bridge flutter analysis (Han *et al.* 2015, Zhang *et al.* 2011) is still based on the linear self-excited forces model established by Scanlan (Scanlan and Tomko 1971). The model is developed by linear vibration theory and the linear self-excited aerodynamic forces expression, and it can be used before the flutter occurs to predict the critical flutter velocity. However, it cannot describe the post-flutter movement.

∗Corresponding author, Professor, E-mail: zhengsx@home.swjtu.edu.cn
[a] Ph.D. Student, Email: guojunfeng_sky@163.com

http://www.techno-press.org/?journal=was&subpage=7 ISSN: 1226-6116 (Print), 1598-6225 (Online)

Many scholars have observed girder movements in post-flutter state. Zhu and Gao (2015) observed some movements of several typical bridge deck cross sections after the flutter occurs by wind tunnel tests, and some scholars called these movements soft flutter. Other scholars, such as Naprstek *et al*. (2007), Amandolese *et al*. (2013), thought them as the phenomenon of nonlinear post-flutter and called them "post critical LCO". Daito *et al*. (2002) also had some findings in wind tunnel tests. For some blunt bridge sections, when the linear aerodynamic negative damping is greater than the structural damping, the "hard flutter" predicted by classic linear theory does not occur. Instead, the flutter is stabilized to a finite amplitude because of the nonlinear effect of self-excited force. Traditional Scanlan's theory cannot fit these recent findings.

Similar phenomenon has been found in the field of aeronautical engineering. For example, Cunningham (2003), Majid and Basri (2008), Tang *et al*. (2003) and Wang and Zha (2011) studied the post-flutter state of aircraft by wind tunnel tests and numerical simulation. Currently, the LCO phenomenon of wings has been well studied. However, in the field of bridge, the phenomenon of soft flutter is less concerned, and the research on it has just risen. The study of the post-flutter state of bridges is of great significance to the more accurate bridge flutter theory and the criterion of bridge flutter stability.

Since the Tacoma bridge accident, some scholars began to try to analyze the large amplitude vibration phenomenon of the bridge. Piccardo (1993) studied the large amplitude phenomenon based on the aerodynamic expression proposed by predecessors, and proposed that the vibration form is a typical limit cycle oscillation. Scanlan (1997) pointed out in his literature that the flutter derivatives are related to the motion amplitude of the bridge deck section, and it told us the linear self-excited model couldn't account for the post-flutter state. Xu and Cao (2001) deduced the nonlinear aerodynamic forces model and got the critical flutter velocity of the Tacoma bridge. In wind tunnel tests, Chen *et al*. (2005), Falco *et al*. (1992), Larose *et al*. (1993), Noda *et al*. (2003) and Wu and Kareem (2013b) studied the aerodynamic self-excited forces by forced vibration method, and the results showed that the self-excited forces acting on bluff bodies are nonlinear and contain obvious higher harmonics. Naprestek (Naprestek *et al*. 2008, Naprestek and Pospíšil 2011) proposed Vanderbilt-Duffen type 2 DOF coupling nonlinear self-excited forces model. Wu and Kareem (2013a) described the nonlinear self-excited forces by Volteria convolution model. Diana *et al*. (2008) proposed the aerodynamic hysteresis of the bridge deck section in his paper, and discussed the aerodynamic hysteresis effect in detail in his subsequent study. In 2010, he studied the nonlinear flutter of the bridge deck section from the energy point of view (Diana *et al*. 2010). Chen and Ma (2011) proposed the application of the Vanderbilt equation to solve the nonlinear aerodynamic forces and explained the soft flutter phenomenon. Wu *et al*. (2013) introduced two advanced nonlinear models, i.e., artificial neural network- (ANN-) and Volterra series-based models to improve the linear and nonlinear aeroelastic analysis frameworks for cable-supported bridges.

Some approaches proposed in above studies (Diana's approach and Wu's approach) can be used in time domain to obtain the post-flutter response, but it is not straightforward or quite complicated to obtain the post-flutter response using those nonlinear approaches. In this paper, the nonlinear self-excited aerodynamic forces and nonlinear flutter derivatives are identified by dynamic mesh technology based on CFD, then they are applied based on the 2 DOF coupling flutter theory so that the traditional linear theory is extended to the nonlinear range, which cannot only calculate the critical state of flutter but also predict the motion state after the flutter occurs.

2. Numerical simulation of bridge aerodynamic self-excited forces

2.1 Description of bridge

A long span suspension bridge with a 1160 m central span length was selected as the research object, and the type of bridge deck is streamlined steel box girder. The span distribution and the bridge deck cross section are shown in Fig. 1. The basic parameters of the streamlined steel box girder in construction state (completely assembled) are shown in Table 1

2.2 Dynamic mesh technology

A computational domain was set, as shown in Fig. 2. The left boundary was the inlet of velocity. The right boundary was the outlet of pressure. The upper and lower boundaries were set as symmetrical boundary conditions. The boundary of the bridge deck cross section was wall. The whole 2D (two-dimensional) wind field was divided into rigid area, deformation area and fixed area from inside to outside. Among them, the rigid area and the bridge deck cross section moved synchronously, the deformation area was refreshed by spring smoothing method, and the fixed area was filled with rigid grid and didn't participate in motion. The numerical wind tunnel simulation was conducted with the FLUENT software in this paper. The calculation parameters were set as follows: velocity of wind flow was U=20 m/s; the SST $k-\omega$ turbulence model was adopted; the turbulence intensity was 0.5%; the turbulence viscosity ratio was 2.

Table 1 Basic parameters of streamlined steel box girder in construction state

Torsional fundamental frequency (Hz)	Vertical fundamental frequency (Hz)	Generalized mass (kg/m)	Generalized mass moment of inertia (kg·m^2/m)
0.3594	0.1686	14215	1372840

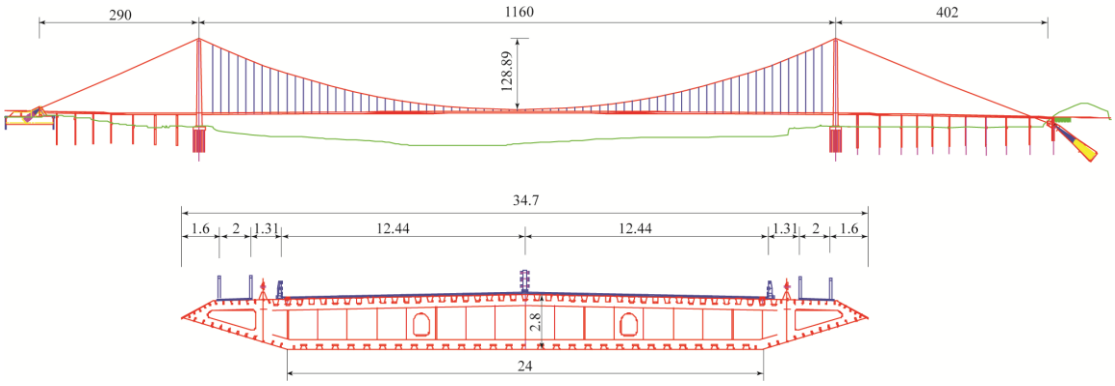

Fig. 1 Arrangement of the bridge span and the bridge deck cross section (unit: m)

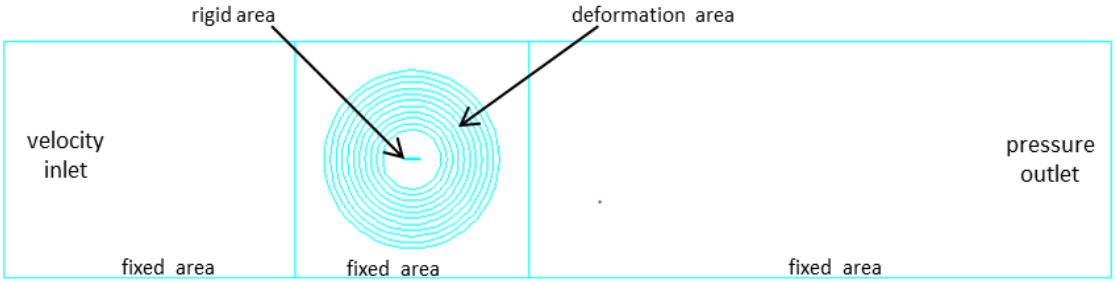

Fig. 2 Computational domain settings

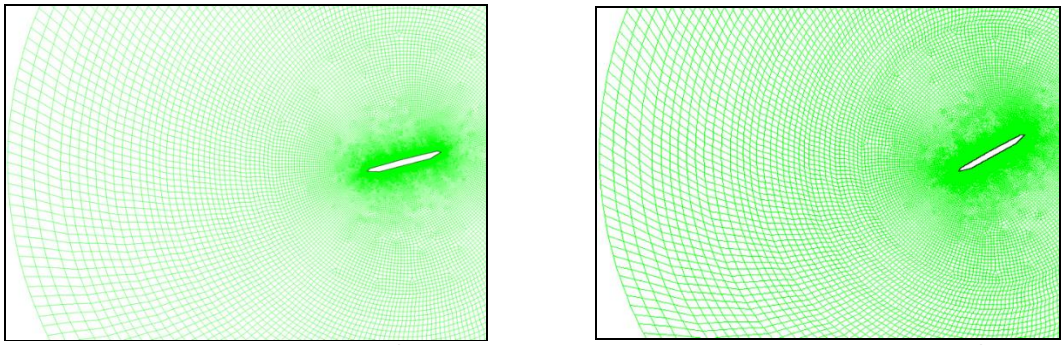

(a) Local mesh deformation under 15° torsional amplitude

(b) Local mesh deformation under 30° torsional amplitude

Fig. 3 Local mesh deformation under large amplitude

The mesh movement can be achieved through self-made user-defined functions (UDF), then it was used in the forced vibration method to identify the aerodynamic self-excited forces. The multi-deformed sub-region dynamic mesh method (The mesh in the deformation area of this method has the control effect of nonlinear spring, which is more suitable for the grid quality in large amplitude motion) would be used because of the large amplitude motion involved in this paper. The deformation area was divided into 10 rings, and the inner side of each ring was prepared with the corresponding UDF to control movement precisely. The rings are of the same frequency vibration with the rigid region form inside to outside, and the ratios of amplitudes of inner sides of rings in deformation area (10 rings from inside to outside) to amplitude of bridge deck model in rigid area are: 1, 0.9, 0.8, 0.7, 0.6, 0.5, 0.4, 0.3, 0.2, and 0.1, respectively. Fig. 3 shows the deformation of local mesh in torsional amplitudes 15° and 30° respectively.

2.3 Identification of nonlinear aerodynamic self-excited forces

According to the CFD method described in section 2.2, a 1:50 model of the bridge deck cross section was built and forced to do single DOF harmonic movement to check the characteristics of the aerodynamic self-excited forces. It should be noted that all of the following analyses are only

for the 0^o initial wind attack angle condition of the bridge deck in construction state, and other conditions have the same principle so that they were not listed one by one. Fig. 4 shows the spectrum characteristics of the aerodynamic self-excited forces with different torsional amplitudes when the initial wind attack angle was 0^o and the reduced wind speed was 5. In the following figures, *Ar* represents the torsional amplitude.

As seen in the Fig. 4, when the reduced wind speed is 5, each harmonic of the aerodynamic self-excited force spectrums (lift spectrum and moment spectrum) is 4.62 Hz, 9.22 Hz and 13.84 Hz respectively. *Ri* = amplitude of higher harmonic / amplitude of fundamental frequency (*i*=*L*, *M*. R_L, is the proportion of lift higher harmonics and R_M is the proportion of moment higher harmonics) was defined to study the variation of higher harmonics with torsional amplitude. Each harmonic can be extracted from Fig.4, then the *Ri* was calculated and the results were plotted in Fig. 5. Fig. 5 shows that: the proportion of second harmonic increases as the torsional amplitude increases when the torsional amplitude is lower than 15^o, but when the torsional amplitude is higher than 15^o, it decreases. However the proportion of third harmonic always increases with the torsional amplitude increases. When the torsional amplitude is higher than 19^o, the proportion of third harmonic is greater than that of second harmonic, and it is consistent with the conclusions obtained by Tang (2015).

In classical linear self-excited force theory, the fundamental frequency amplitude of aerodynamic self-excited forces increases as the torsional amplitude increases, and the two should be linear. But when the reduced wind speed is high or the torsional amplitude is large, the two may be nonlinear. To explain the phenomenon, the fundamental frequency amplitudes of aerodynamic self-excited forces of streamlined steel box girder were plotted in Fig. 6 when the reduced wind speed was 16. The dotted straight line in this figure was determined by the coordinate origin and the fundamental frequency amplitude of 2^o torsional amplitude. So all the points in this dotted straight line indicate the linear aerodynamic self-excited forces fundamental frequency amplitude (referred as theoretical linear value in the following sections) in classical linear self-excited force theory. The discrete black dots in the graph represent the actual fundamental frequency amplitudes corresponding to different torsional amplitudes based on the CFD, and a curve was fitted by these dots so that all the points in this curve represent the actual fundamental frequency amplitude (referred as actual value in the following sections).

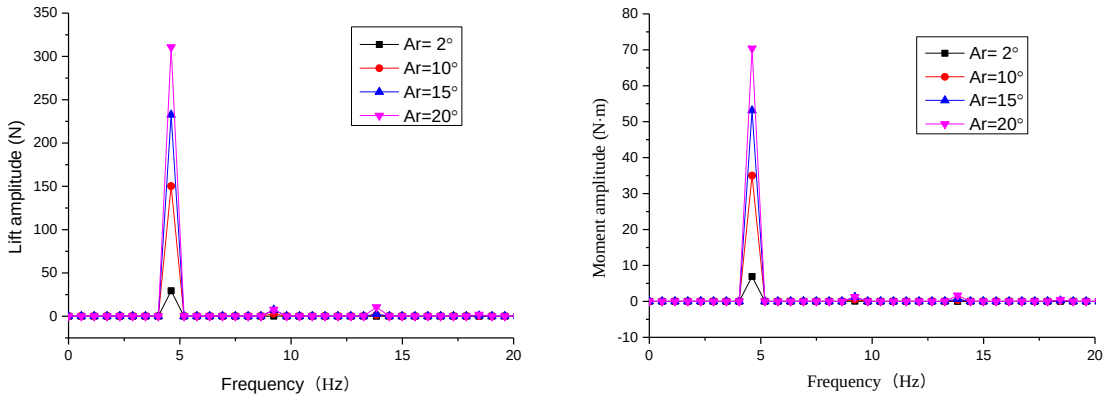

(a) Lift spectrum (b) Moment spectrum

Fig. 4 Aerodynamic self-excited force spectrum of streamlined steel box girder

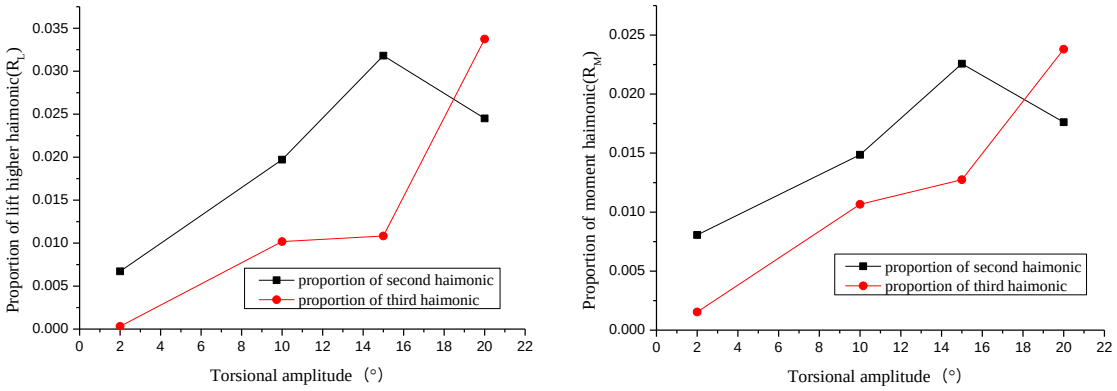

(a) R_L (b) R_M

Fig. 5 The relationship between proportion of aerodynamic self-excited force higher harmonic and torsional amplitude

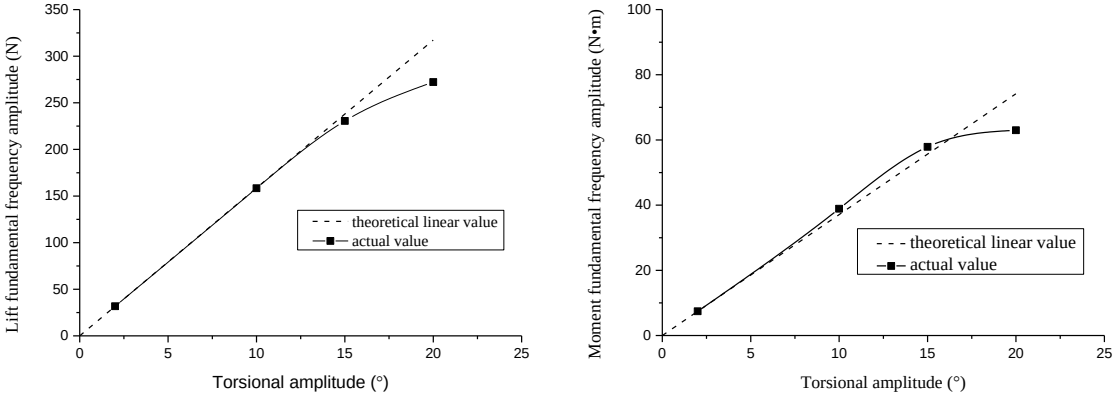

(a) The relationship between lift fundamental frequency amplitude and torsional amplitude

(b) The relationship between moment fundamental frequency amplitude and torsional amplitude

Fig. 6 The relationship between aerodynamic self-excited forces fundamental frequency amplitude and torsional amplitude

It is worth noting that, for simplicity, only four points are used to fit curve in Fig. 6. Thus, the critical values between linear curve and nonlinear curve (7^o, 13^o and 16^o proposed below) are approximate values rather than exactly accurate values. But they can still be used to explain the nonlinear effect adequately under the large torsional amplitude. As can be seen from Fig. 6, when the torsional amplitude was less than 13^o, the actual value of aerodynamic lift overlapped with the theoretical linear value. But when the torsional amplitude was greater than 13^o, the actual value is smaller than the theoretical linear value. Meanwhile the distance between actual value and theoretical linear value is greater as the torsional amplitude increased, and at this point the relationship between aerodynamic lift and torsional amplitude was not linear. For the aerodynamic

moment, the actual value almost overlapped with the theoretical linear value when the torsional amplitude was less than 7^o and the relationship between aerodynamic moment and torsional amplitude was linear; the actual value started to deviate upward from the theoretical linear value when the torsional amplitude was in the range of 7^o to 16^o and the actual value started to deviate downward from the theoretical linear value when the torsional amplitude was greater than 16^o. In general, the aerodynamic lift amplitude of fundamental frequency and the aerodynamic moment amplitude of fundamental frequency were only linearly related to the torsional amplitude at a small amplitude (13^o and $7^{o)}$; If the actual value is replaced by the theoretical linear value under the large torsional amplitude, it would result errors in computation.

Flutter occurs when the torsional damping of the bending and torsional coupling motion changes from positive to negative in linear aerodynamic self-excited forces theory. But in fact, the aerodynamic self-excited forces do not change linearly as the torsional amplitude increases. The decrease of the aerodynamic lift and the increase of the aerodynamic moment may cause the torsional damping ratio of the bending and torsional coupling motion changes from negative to positive. So the linear aerodynamic self-excited forces theory is not suitable at this point.

3. Identification of nonlinear flutter derivatives

3.1 Basic assumption

At present, most scholars think that the motion form of girder section in the post flutter state is a single frequency vibration coupled with torsional and vertical DOF. Some scholars have observed this phenomenon in wind tunnel tests and numerical wind tunnels. Zhu and Gao (2015) observed that the soft flutter response of four typical girder sections has this feature. Ying et al. (2016) and Zhang *et al.* (2016) set a fluid-structure interaction model with FLUENT to study soft flutter characteristics of girder section and found the same feature too. They also found that the frequency decreases as the wind speed increases. Therefore, it was assumed that the motion pattern of the streamlined steel box girder in post flutter state is also the bending and torsion coupling single-frequency vibration. The assumption would be verified by wind tunnel tests in section 5.

Under this assumption, only the fundamental frequency component of movement is considered. The aerodynamic forces with high frequency got in section 2.3 did no work on the fundamental frequency component of girder movement (Tang 2015). So only the fundamental frequency part of aerodynamic self-excited forces need to be considered in the identifications of nonlinear flutter derivatives. This method has the same form with the traditional linear flutter derivatives identification method, but the nonlinear flutter derivatives are related to the reduced wind speed and they are the nonlinear function of torsional amplitude. We can also call them 3D flutter derivatives.

3.2 Nonlinear flutter derivatives

As can be seen from the previous section, forced vibration method can be used in the identification of the nonlinear flutter derivatives similar to the linear flutter derivatives. But the difference is that the nonlinear flutter derivatives are not only related to reduced wind speed, but also torsional and vertical amplitudes. In order to be distinguished from the traditional linear flutter derivatives, eight symbols of nonlinear flutter derivatives were defined ($H_i^{\#}$, $A_i^{\#}$, i=1 , 2 , 3 ,

4). $H_i^{\#} = f(V_r, A_r), A_i^{\#} = f(V_r, H_r)$ *Vr* is reduced wind speed , *Ar* is torsional amplitude , *Hr*=vertical amplitude/B. B is width of bridge deck model. (the geometric ratio of model is 1/40). The test parameters on CFD are listed in Table 2. The number of mesh is about 440000. And the tested motion amplitudes as follow:

(1) For vertical motion:

The tested vertical amplitudes are: 0.001B, 0.003B, 0.007B, 0.01B, 0.012B, 0.015B, 0.02B, 0.03B, 0.04B, 0.05B, 0.06B, 0.07B, 0.08B, 0.09B, 0.1B, 0.11B, 0.12B, 0.13B, 0.14B, 0.15B, 0.18B, 0.20B.

(2) For torsional motion:

The tested torsional amplitudes are: 0.1°, 0.3°, 0.7°, 1.2°, 1.6°, 2°, 3°, 4°, 5°, 7°, 10°, 13°, 15°, 18°, 20°, 23°, 25°, 27°, 30°.

"Least-squares method" is used to obtain the flutter derivatives from self-excited forces in this paper. Then the nonlinear flutter derivatives had been identified and displayed in Figs. 7 and 8.

It can be seen from Figs. 7 and 8 that the sensitivity of the different 3D flutter derivative surface is different for amplitude. Changes in the nonlinear flutter derivatives, $H_1^{\#}$, $H_4^{\#}$, $A_1^{\#}$ and $A_4^{\#}$,which are related to the vertical vibration, are small with the amplitude. Their 3D surfaces can be seen as 2D flutter derivatives curve sweep along the amplitude direction evenly. So the influence of the vertical motion amplitude on the nonlinear flutter derivatives can be neglected. Changes in the nonlinear flutter derivatives, $H_2^{\#}$, $H_3^{\#}$, $A_2^{\#}$ and $A_3^{\#}$, which are related to the torsional vibration, are large with the amplitude. Their 3D surfaces have significant changes in 15^o-20^o. So the torsional amplitude has a great influence on the nonlinear flutter derivatives. Therefore, the following analysis of the post-flutter state should take the effect of the motion amplitudes (torsional and vertical amplitudes) into account.

Table 2 The test parameters on CFD

The reduced wind speed	The frequencies of the imposed motion (Hz)	The corresponding dimensionless time-step
2	11.5327	0.0008671
3	7.6885	0.00130065
4	5.7663	0.0017342
5	4.6131	0.00216775
6	3.8442	0.0026013
7	3.2951	0.00303485
8	2.8832	0.0034684
9	2.5628	0.00390195
10	2.3065	0.0043355

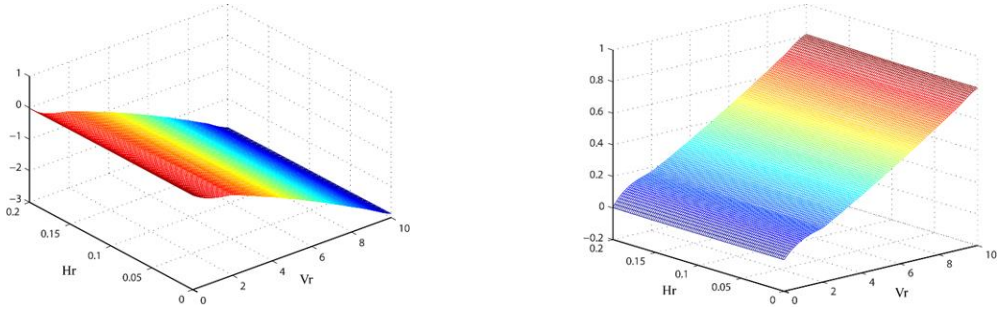

(a) $H_1^{\#}$ (b) $A_1^{\#}$

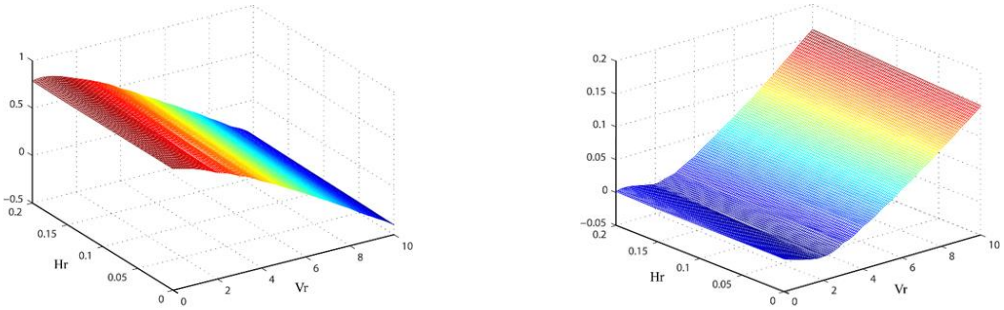

(c) $H_4^{\#}$ (d) $A_4^{\#}$

Fig. 7 3D flutter derivative surface of streamlined steel box girder (vertical motion)

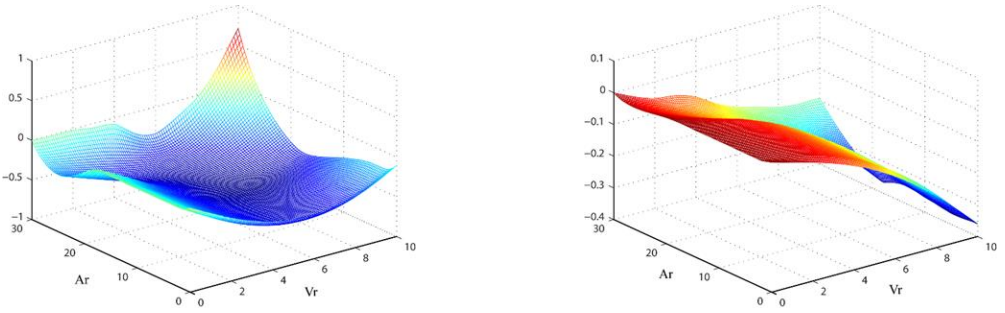

(a) $H_2^{\#}$ (b) $A_2^{\#}$

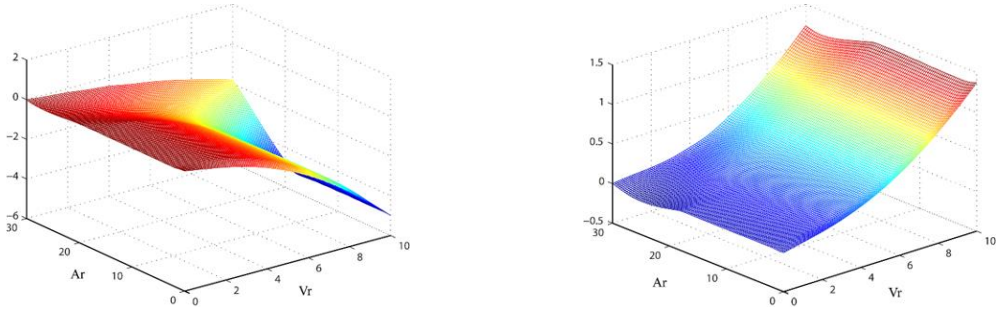

(c) $H_3^{\#}$ (d) $A_3^{\#}$

Fig. 8 3D flutter derivative surface of streamlined steel box girder (torsional motion)

4. Post-flutter state analysis method based on 2D flutter frequency domain iteration method

4.1 Improved 2D direct calculation method for bridge flutter

In the classical flutter theory, flutter is a divergent self-excited vibration with the interaction of wind and structure. Long span bridges are long and slender structures whose geometric scales tend to be large in one direction and small in the other two directions. The effect of wind on the structure can be expressed in terms of strip theory. Therefore, the 2D direct analysis method and the section model wind tunnel tests are common research methods in bridge flutter analysis.

However, the traditional 2D direct calculation method is developed by linear flutter theory, which does not consider the changes of flutter derivatives with amplitude. In particular, the effect of torsional amplitude on the 3D flutter derivatives is large, and this effect cannot be neglected. Therefore, the 3D flutter derivatives identified in Section 3.2 were introduced into the traditional 2D direct calculation method and the nonlinear changes of the flutter derivatives with amplitude were considered in the linear flutter theory. The flutter derivatives were regarded as the binary function of the reduced wind speed and amplitude. So they can not only calculate the critical state of flutter, but also predict the movement in post-flutter state by modifying the 2D direct method. Specific derivation is as follows.

Generally, torsional DOF α and vertical DOF h are considered in 2D flutter analysis model, the equation of motion is

$$\begin{cases} m\ddot{h} + 2\xi_h \omega_h m\dot{h} + m\omega_h^2 h = L \\ I_t\ddot{\alpha} + 2\xi_t \omega_t I_t\dot{\alpha} + I_t\omega_t^2\alpha = M \end{cases} \tag{1}$$

Where m, I_t are mass and moment of inertia per meter of section model, respectively; ω_h, ω_t are circle frequency of bending and torsion vibration, respectively; ξ_h, ξ_t are the damping ratio of bending and torsion, respectively; L, M are lift and moment of lift per meter of section model, respectively.

Scanlan's aerodynamic self-excited forces expression in frequency domain were introduced

$$\begin{cases} L = \frac{1}{2}\rho U^2(2B)[KH_1^{\#}\frac{\dot{h}}{U} + KH_2^{\#}\frac{B\dot{\alpha}}{U} + K^2H_3^{\#}\alpha + K^2H_4^{\#}\frac{h}{B}] \\ M = \frac{1}{2}\rho U^2(2B^2)[KA_1^{\#}\frac{\dot{h}}{U} + KA_2^{\#}\frac{B\dot{\alpha}}{U} + K^2A_3^{\#}\alpha + K^2A_4^{\#}\frac{h}{B}] \end{cases} \tag{2}$$

Where ρ is air density; U is average wind speed; B is bridge width; h, α are vertical displacement and torsional displacement, respectively; $H_i^{\#}, A_i^{\#}$ are nonlinear flutter derivatives of bending and torsion, respectively.

To simplify the formula, self-excited forces were simplified as follows

$$\begin{cases} L = H_1\dot{h} + H_2\dot{\alpha} + H_3\alpha + H_4 h \\ M = A_1\dot{h} + A_2\dot{\alpha} + A_3\alpha + A_4 h \end{cases} \tag{3}$$

Where H_i, A_i (i=1, 2, 3, 4) are dimensional nonlinear flutter derivatives. They are the

combi-nation of factors and nonlinear flutter derivatives. The difference from the traditional solut-ion is that H_i and A_i are not only related to the reduced wind speed, but also to the a-mplitude. They are nonlinear functions of motion amplitude.

Substituting Eq. (3) into Eq. (1), the next equation was got

$$\begin{pmatrix} \ddot{h} \\ \ddot{\alpha} \end{pmatrix} + \begin{pmatrix} 2\xi_h\omega_h - \frac{H_1}{m} & -\frac{H_2}{m} \\ -\frac{A_1}{I} & 2\xi_\alpha\omega_\alpha - \frac{A_2}{I} \end{pmatrix} \begin{pmatrix} \dot{h} \\ \dot{\alpha} \end{pmatrix} + \begin{pmatrix} \omega_h^2 - \frac{H_4}{m} & -\frac{H_3}{m} \\ -\frac{A_4}{I} & \omega_\alpha^2 - \frac{A_3}{I} \end{pmatrix} \begin{pmatrix} h \\ \alpha \end{pmatrix} = 0 \tag{4}$$

Using the matrix notation to change the above formula to

$$[I]\begin{pmatrix} \ddot{h} \\ \ddot{\alpha} \end{pmatrix} + [A]\begin{pmatrix} \dot{h} \\ \dot{\alpha} \end{pmatrix} + [B]\begin{pmatrix} h \\ \alpha \end{pmatrix} = 0 \tag{5}$$

Where [*I*] is a second order diagonal identity matrix. The definition of [*A*] and [*B*] can be got bycomparing Eq. (4) with Eq. (5).

The above equation was rewritten as a first order differential equation group with $x = \dot{h}$ and $y = \dot{\alpha}$.

$$\begin{pmatrix} 0 & I \\ I & A \end{pmatrix} \begin{pmatrix} \dot{x} \\ \dot{y} \\ \dot{h} \\ \dot{\alpha} \end{pmatrix} + \begin{pmatrix} -I & 0 \\ 0 & B \end{pmatrix} \begin{pmatrix} x \\ y \\ h \\ \alpha \end{pmatrix} = 0 \tag{6}$$

Where each sub-matrix is a 2×2 matrix, 0 represents a zero matrix.

Since (6) can uniquely determine the motion state of the 2 DOF system, so the equatio-n is called the state equation. $(x, y, h, \alpha)^T$ is the state vector.

The structure flutters with equal frequency when wind speed comes to the critical flutte-r velocity. So we can assume that

$$\begin{pmatrix} x \\ y \\ h \\ \alpha \end{pmatrix} = \begin{pmatrix} x_0 \\ y_0 \\ h_0 \\ \alpha_0 \end{pmatrix} e^{i\omega t} \tag{7}$$

Where ω is a real number. Substituting Eq. (7) into Eq. (6), the next equation is got

$$\left\{ i\omega \begin{pmatrix} 0 & I \\ I & A \end{pmatrix} \begin{pmatrix} x_0 \\ y_0 \\ h_0 \\ \alpha_0 \end{pmatrix} + \begin{pmatrix} -I & 0 \\ 0 & B \end{pmatrix} \begin{pmatrix} x_0 \\ y_0 \\ h_0 \\ \alpha_0 \end{pmatrix} \right\} e^{i\omega t} = 0 \tag{8}$$

The above equation is satisfied for any $e^{i\omega t}$, so

$$\begin{pmatrix} -I & i\omega I \\ i\omega I & i\omega A+B \end{pmatrix} \begin{pmatrix} x_0 \\ y_0 \\ h_0 \\ \alpha_0 \end{pmatrix} = 0 \tag{9}$$

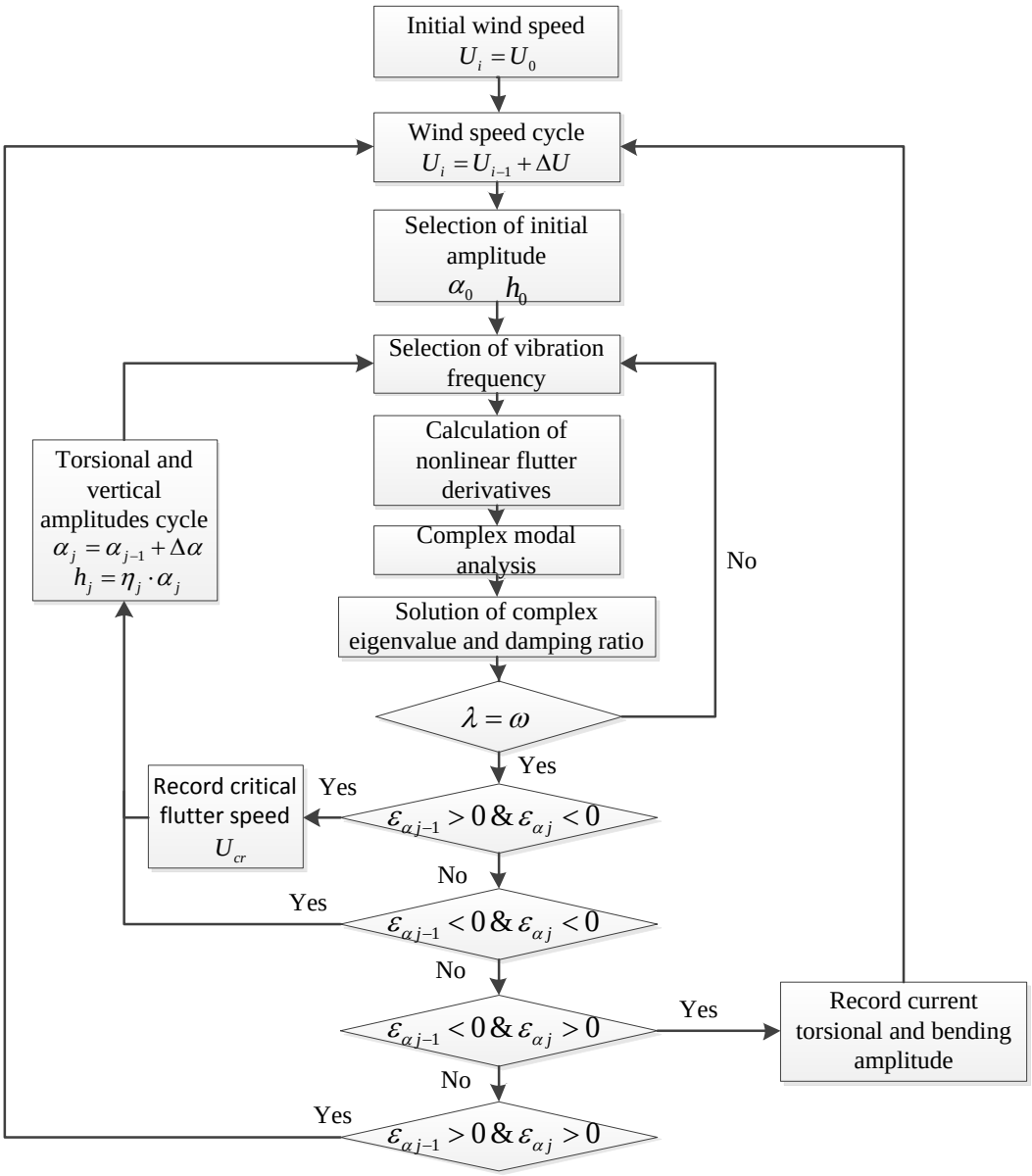

Fig. 9 Flow chart for post flutter analysis program

If Eq. (9) has a nonzero solution, its coefficient determinant must be zero. The coefficient determinant of Eq. (9) is a fourth-order differential equation with ω, called the characteristic equation. The equation has two unknown variables, ω and U. The nonlinear flutter derivatives are related to the torsional and vertical amplitudes. So in the process of calculation, a double cycle of motion amplitudes and wind speed is required. Firstly, the nonlinear flutter derivatives of initial motion amplitudes and the initial wind speed value were substituted into the coefficient matrix and four roots of ω were got by the complex coefficient matrix eigenvalue method. If one of the four roots is a real number, this root is the vibration frequency of critical flutter state. The corresponding wind speed is the critical flutter velocity and the corresponding motion amplitudes are the steady-state response amplitudes of flutter. If there is no real number in the four roots, then go to the next loop until all critical flutter velocity and the steady-state response amplitude of flutter are found. If no appropriate motion amplitudes and wind speed can be obtained to calculate the critical flutter velocity and the steady-state response amplitudes of flutter, it is the state of flutter divergence. In order to solve the characteristic equation of Eq. (9), a double search for critical flutter velocity and the steady-state response amplitudes of flutter can be achieved with the help of computer program. It is worth noting that the ratio (η) of vertical amplitude to torsional amplitude need be calculated before running the post-flutter analysis program, since motion amplitudes (torsional and vertical amplitudes) are involved in it. The four roots of ω are substituted to Eq. (9) to get corresponding complex eigenvector by which equation of motion can be obtained. Then the ratio (η) can be obtained from the flutter mode of vibration. A flow chart for the above proposed method is shown in Fig. 9. The meaning of some key signs in Fig. 9 is that: λ is the eigenvalue of characteristic matrix; ω is vibration frequency; ε_{α_j} is the jth torsional damping ratio; η_i is the jth ratio of vertical amplitude to torsional amplitude.

4.2 Results analysis

The post-flutter state analysis program as shown in Fig. 9 was compiled with MATLAB. The basic parameters of the streamlined steel box girder displayed in section 2.1 and the nonlinear flutter derivatives obtained in section 3.2 were substituted into the analysis program. Setting two damping ratios (damping ratio 0.3% and 0.6%) to run the above program, respectively. The results are shown in Fig. 10.

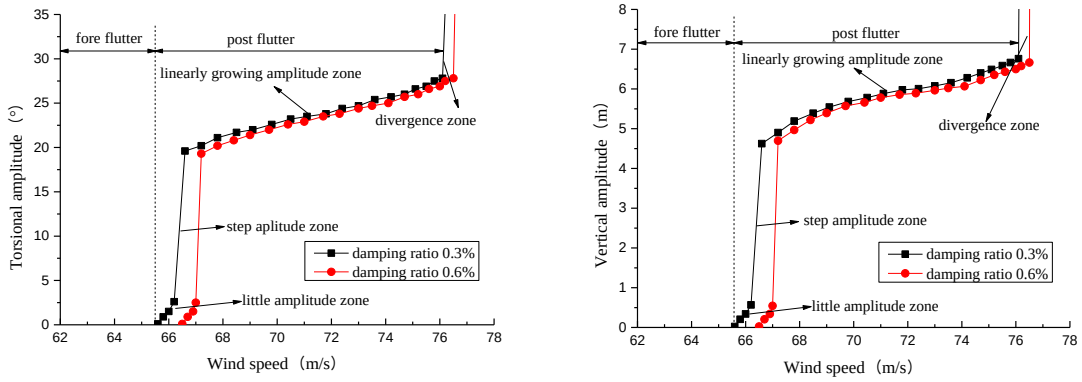

(a) Torsional movement (b) Vertical movement

Fig. 10 Displacement response of streamlined steel box girder in post flutter

Analyzing the torsional motion curve with the damping ratio of 0.3% in Fig. 10(a) (the rest of the curves can be analyzed in the same way), we can find that: the critical flutter velocity is 65.6 m/s, but when the wind speed is just a little higher than 65.6 m/s, the torsional amplitude was not infinitely divergent and the bridge did not lose stability immediately. Instead, the amplitude had a gradual increase when wind speed in the range of 65.6 m/s to 66.2 m/s. Since the bridge was not destroyed in the wind speed range of the small amplitude, this wind speed range was defined as " little amplitude zone ".When the wind speed exceeds 66.2 m/s to 66.6 m/s, the torsional amplitude will appear a jump, and directly to 19.6^{o} and the wind speed range was defined as the "step amplitude zone". It should be noted that the discussion of the displacement response here refers to the flutter steady-state response. It means that when the wind speed increased from 66.2 m/s to 66.6m/s, the torsional amplitude did not jump directly to 19.6^{o}, but gradually increased to 19.6^{o} through oscillation with continuously absorbing energy from wind. Then a new balance was achieved when the amplitude was 19.6^{o}. When the wind speed was in the range of 66.6 m/s to 76.1 m/s, the flutter amplitude increased with the increase of the wind speed, and the two are linear in general. This wind speed range was defined as "linearly growing amplitude zone". The amplitude began to infinitely grow, eventually leading to flutter divergence until wind speed exceeds 76.1 m/s.

Comparing the two torsional vibration curves with the damping ratios of 0.3% and 0.6% in Fig. 10(a) (Fig. 10(b) similarly), we can find that increasing the damping ratio is equivalent to moving the whole curve to the right. Therefore, increasing the damping ratio can improve the critical flutter velocity and the divergent flutter velocity. But the improvement is very limited. The improvement of critical flutter velocity was only 0.9 m/s and that of divergent flutter velocity was only 0.4 m/s when the damping ratio was increased by 0.3%. In terms of the flutter response amplitude, increasing the damping ratio can slightly reduce the amplitude of the flutter steady-state response.

5. Section model test validation

5.1 Test parameters

In order to test the rationality of the theory and the results mentioned above, a section model test was designed to verify them. The test was carried out in the high speed test section of the wind tunnel XNJD-1. The test section has a rectangular cross section with size of 2.4 m (width) X 2.0 m (height). The section model was made by a 1:40 scale ratio with the considerations of the actual size of girder cross section, the size of the wind tunnel and test requirements. The section model was suspended by eight pairs of tension springs, as shown in Fig. 11 below.

5.2 Analysis of test results

5.2.1 Effect of damping ratio

In order to maintain consistency with the foregoing, the same two damping ratios were set in the test. Fig. 12 shows the changes of the torsional and vertical response of the streamline steel box girder with wind speed under the condition of different damping ratios. Limited to the wind tunnel test device, the test can't detect the large amplitude movement of the girder. Therefore, this test only gave the results of "little amplitude zone" in the post-flutter state.

Fig. 11 Section model in wind tunnel

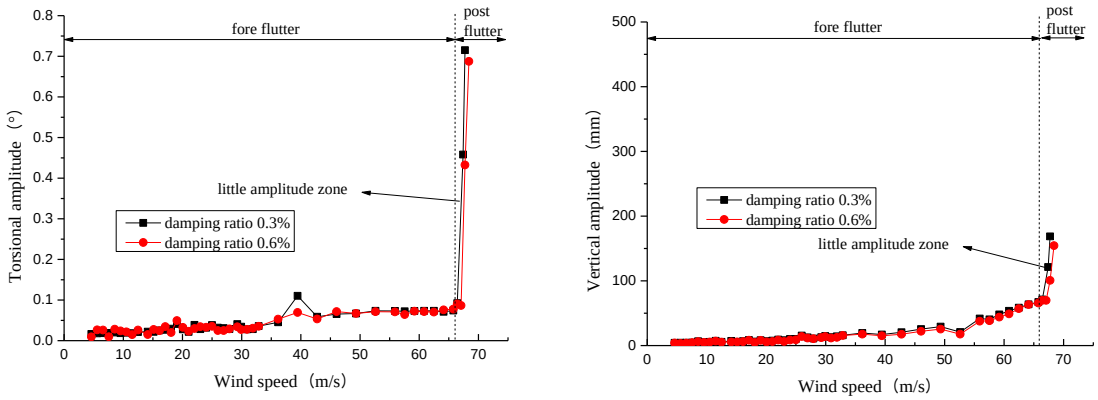

(a) Torsional movement (b) Vertical movement

Fig. 12 Displacement response of streamlined steel box girder in wind tunnel

The torsional vibration curve with the damping ratio of 0.3% in Fig. 12(a) was analyzed (the rest of the curves can be analyzed in the same way). Then it can be found that the streamlined steel box girder did not lose stability immediately when the wind speed just reached the critical flutter velocity. As predicted by previous numerical simulations, there is also a " little amplitude zone ". The wind speed range is 66.42 m/s to 67.74 m/s and there is a certain discrepancy in test results compared with the value of 65.6 m/s to 66.4 m/s in previous calculation. But this discrepancy is small and unavoidable. There are probably two reasons for this discrepancy: the first is the system and random discrepancy that cannot be avoided during the wind tunnel tests; the other is that the numerical simulation does not completely simulate the real situation of the wind tunnel.

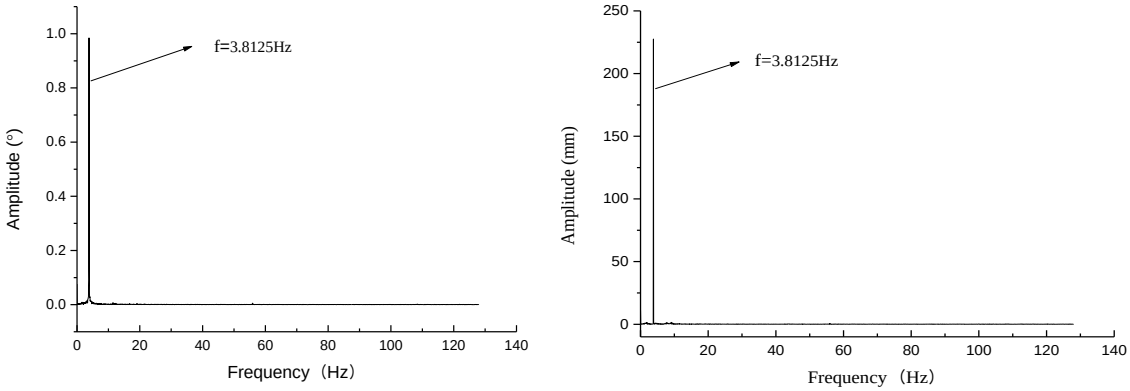

(a) Torsional displacement (b) Vertical displacement

Fig. 13 Displacement response spectrum of post flutter in wind tunnel

The same conclusion as the previous numerical method can be obtained by comparing the two torsional vibration curves with the damping ratio of 0.3% and 0.6% in Fig. 12(a). Increasing the damping ratio can improve the critical flutter velocity but the improvement is very limited.

Comparing numerical results (Fig. 10) with the test results (Fig. 12) comprehensively, we can see that the two are in good agreement with the same law. It prove that the method proposed in this paper is reasonable.

5.2.2 Vibration characteristics in post-flutter state

A torsional vibration curve and a vertical vibration curve with a damping ratio of 0.3% in Figs. 12(a) and 12(b) were selected. Then the torsional vibration time-history curve and the vertical bending time-history curve of the two points (where wind speed is 67.74 m/s), which is located in "little amplitude zone", were transformed by FFT (Fast Fourier Transform) to get the displacement response spectrum in post-flutter state as shown in Fig. 13.

It can be seen that the torsional vibration and the vertical vibration are single-frequency vibrations when the wind speed exceeds the critical flutter velocity, and the two will be coupled into the same frequency for single-frequency harmonic vibration. This test verifies the assumption presented in section 3.1.

6. Conclusions

Based on the CFD, the nonlinear aerodynamic self-excited forces of the streamlined steel box girder were calculated. Then the nonlinear flutter derivatives were identified. The amplitude and the nonlinear flutter derivatives that change with amplitude were introduced into the traditional 2D flutter iterative method in frequency domain, and the program was modified accordingly, so that the improved method (post-flutter analysis program) can achieve a double search of the critical flutter velocity and the amplitude in post-flutter state. Finally, the corresponding wind tunnel test was set up to verify the rationality of the analytical method described in this paper. We got the following conclusions:

- There are four phases in post-flutter state of streamlined steel box girder with the increase of wind speed. They are "little amplitude zone", "step amplitude zone", "linearly growing amplitude zone" and "divergence zone".
- The damping ratio has a very limited effect on the critical flutter velocity and the stable response in post-flutter state of streamlined steel box girder.
- After the flutter occurs, the torsional vibration and the vertical vibration will be coupled into the same frequency to do single-frequency harmonic vibration.
- Different 3D flutter derivative surfaces have different sensitivity to the motion amplitude. The effect of the vertical amplitude on the nonlinear flutter derivatives can be negligible, and the torsional amplitude has a great influence on the nonlinear flutter derivatives.
- When the reduced wind speed is large, the amplitude of the fundamental frequency of the aerodynamic self-excited force is nonlinearly related to the torsional amplitude, and the larger the torsional amplitude is, the greater the difference between the theoretical linear value and the actual value.

Acknowledgments

The research described in this paper was financially supported by the Natural Science Foundation of China under grant number 51378443**,** the Joint Funds of National Natural Science of China and High-Speed Railway under grant number U1434205. This support is much appreciated. The valuable comments of the anonymous reviewers of the paper are also acknowledged.

References

Amandolese, X., Michelin, S. and Choquel, M. (2013), "Low speed flutter and limit cycle oscillations of a two-degree-of-freedom flat plate in a wind tunnel", *J. Fluid. Struct.*, **43**(6), 244-255.

Chen, A. and Ma, R. (2011), "Self-excited force model and parameter identification for soft flutter", *Proceedings of the International Conference of Wind Engineering*. Amsterdam, Netherlands, July.

Chen, Z.Q., Yu, X.D., Yang, G. and Spencer, Jr. B.F. (2005), "Wind-induced self-excited loads on bridges", *J. Struct. Eng.*, **131**(12), 1783-1793.

Cunningham, A.M. (2003), "Buzz, buffet and LCO on military aircraft–the aeroelastician's nightmares", *Proceedings of the International Forum on Aeroelasticity and Structural Dynamics*, Amsterdam, Netherlands, June.

Daito, Y., Matsumoto, M. and Araki, K. (2002), "Torsional flutter mechanism of two-edge girders for long-span cable-stayed bridge", *J. Wind Eng. Ind. Aerod.*, **90**(12), 2127-2141.

Diana, G., Resta, F. and Rocchi, D. (2008), "A new numerical approach to reproduce bridge aerodynamic non-linearities in time domain", *J. Wind Eng. Ind. Aerod.*, **96**(10), 1871-1884.

Diana, G., Rocchi, D., Argentini, T. and Muggiasca, S. (2010), "Aerodynamic instability of a bridge deck section model: Linear and nonlinear approach to force modeling", *J. Wind Eng. Ind. Aerod.*, **98**(6), 363-374.

Falco, M., Curami, A. and Zasso, A. (1992), "Nonlinear effects in sectional model aeroelastic parameters identification", *J. Wind Eng. Ind. Aerod.*, **42**(1-3), 1321-1332.

Han, Y., Liu, S. and Cai, C.S. (2015), "Flutter stability of a long-span suspension bridge during erection", *Wind Struct.*, **21**(1), 41-61.

Larose, G.L., Davenport, A.G. and King, J.P.C. (1993), "On the unsteady aerodynamic forces on a bridge

deck in turbulent boundary layer flow", *Proceedings of the 7th U.S. National Conference on Wind Engineering*, pages 373-382, UCLA, Los Angeles, CA. G.C. Hart.

Majid, D.L.A.H.A. and Basri, S. (2008), "LCO flutter of cantilevered woven glass/epoxy laminate in subsonic flow", *Acta Mechanica Sinica*, **24**(1), 107-110.

Náprstek, J. and Pospíšil, S. (2011), "Post-critical behavior of a simple non-linear system in a cross-wind", *Eng. Mech.*, **18**(3-4), 193-201.

Náprstek, J., Pospíšil, S. and Hračov, S. (2007), "Analytical and experimental modelling of non-linear aeroelastic effects on prismatic bodies", *J. Wind Eng. Ind. Aerod.*, **95**(9), 1315-1328.

Náprstek, J., Pospıšil, S., Höffer, R. and Sahlmen, J. (2008), "Self-excited nonlinear response of a bridge-type cross section in post-critical state", *Proceedings of the 6th International Colloquium on Bluff Body Aerodynamics and Applications*, Milano, Italy, July.

Noda, M., Utsunomiya, H., Nagao, F., Kanda, M. and Shiraishi, N. (2003), "Effects of oscillation amplitude on aerodynamic derivatives", *J. Wind Eng. Ind. Aerod.*, **91**(1), 101-111.

Piccardo, G. (1993), "A methodology for the study of coupled aeroelastic phenomena", *J. Wind Eng. Ind. Aerod.*, **48**(2-3), 241-252.

Scanlan, R.H. (1997), "Amplitude and turbulence effects on bridge flutter derivatives", *J. Struct. Eng.*, **123**(2), 232-236.

Scanlan, R.H. and Tomko, J.J. (1971), "Air foil and bridge deck flutter derivatives", *J. Eng. Mech. - ASCE*, **97**(6), 1717-1737.

Tang, L., Bartels, R.E., Chen, P.C. and Liu, D.D. (2003), "Numerical investigation of transonic limit cycle oscillations of a two-dimensional supercritical wing", *J. Fluid. Struct.*, **17**(1), 29-41.

Tang, Y. (2015), "Nonlinear self-excited forces of streamlined box deck and nonlinear flutter response", Ph.D. Dissertation, Southwest Jiaotong University, Chengdu, China.

Wang, B. and Zha, G.C. (2011), "Detached-eddy simulation of transonic limit cycle oscillations using high order schemes", *Comput. Fluid.*, **52**, 58-68.

Wu, T. and Kareem, A. (2013a), "A nonlinear convolution scheme to simulate bridge aerodynamics", *Comput. Struct.*, **128**, 259-271.

Wu, T. and Kareem, A. (2013b). "Aerodynamics and Aeroelasticity of Cable-Supported Bridges: Identification of Nonlinear Features", *J. Eng. Mech. – ASCE*, **139**(12), 1886-1893.

Wu, T., Kareem, A. and Ge, Y. (2013), "Linear and nonlinear aeroelastic analysis frameworks for cable-supported bridges", *Nonlinear Dynam.*, **74**(3), 487-516.

Xu, X. and Cao, Z.Y. (2001), "Linear and nonlinear aerodynamic theory of interaction between flexible long structure and wind", *Appl. Math. Mech.*, **22**(12), 1446-1457.

Ying, X.Y., Xu, F.Y. and Zhang, Z. (2016), "Study on numerical simulation and mechanism of soft flutter of a bridge deck". *Proceedings of the ACEM*. Jeju, Koraea, September.

Zhang, M.J., Xu, F.Y. and Ying, X.Y. (2016), "Experimental investigations on the soft flutter of a bridge deck", *Proceedings of the ACEM*. Jeju, Koraea, September.

Zhang, W.M., Ge, Y.J. and Levitan, M.L. (2011), "Aerodynamic flutter analysis of a new suspension bridge with double main spans", *Wind Struct.*, **14**(3), 187-208.

Zhu, L.D. and Gao, G.Z. (2015), "Influential factors of soft flutter phenomenon for typical bridge deck sections", *J. Tongji University (Natural science)*, **43**(9), 1289-1294. In Chinese.

AD